Tectonophysics, 198 (1991) 23–34
Elsevier Science Publishers B.V., Amsterdam

Fluid evolution history of brittle–ductile shear zones on the hanging wall of Yellow Spring thrust, Valley and Ridge Province, Pennsylvania, U.S.A.

D.C. Srivastava [1] and Terry Engelder

Department of Geosciences, The Pennsylvania State University, University Park, PA 16802, USA

(Received October 2, 1989; revised version accepted March 13, 1991)

ABSTRACT

Srivastava, D.C. and Engelder, T., 1991. Fluid evolution history of brittle–ductile shear zones on the hanging wall of Yellow Spring thrust, Valley and Ridge Province, Pennsylvania, U.S.A. *Tectonophysics*, 198: 23–34.

This work presents the results of structural and fluid inclusion analyses of brittle–ductile shear zones (bdsz) cutting Lower Paleozoic carbonates in the Appalachian fold and thrust belt. Strike parallel extension of the beds riding up the ramp of Yellow Spring thrust resulted in development of conjugate bdsz by progressively non-coaxial deformation. During the shearing, syntectonic extension veins were formed by successive episodes of mode-I cracking and sealing by the precipitation of quartz, saddle dolomite and calcite in paragenetic order. Geobarometry on co-existing methane-rich and water-rich fluid inclusions reveals the trapping of fluids at large range of fluid pressures. The values of maximum and minimum fluid pressures correspond to the events of crack propagation and complete sealing respectively. Contrary to ductile shear zones in high-grade metamorphic rocks, this study in unmetamorphosed rocks shows that bdsz evolve by influx of locally derived methane bearing brines of connate or evolved formation water origin at pressures of 80–40 MPa, temperatures of 155–165 °C and a depth of 6 km. It is shown that the salinity and composition of the mineralizing fluids change from one crack-seal episode to another, in spite of a broad consistency in the pressure–temperature conditions.

Introduction

Shear zones ranging from brittle faults to concentrated ductile flow zones (Ramsay, 1980a) are one of the most common consequences of crustal deformation in rocks of diverse metamorphic grade and tectonic frame work. Furthermore, shear zones also represent most conspicuous examples of large fluid fluxes during deformation. In particular, brittle–ductile shear zones containing hydraulic fractures (mode-I cracks Pollard and Aydin, 1988) and syntectonic extension veins, are the immediate examples of enhanced permeability and fluid flow during deformation in natural rocks. These syntectonic fluids are often preserved as fluid inclusions in extension veins of shear zones. In this paper, we focus on construing a pressure–temperature (P–T) history of fluids during the development of outcrop scale shear zones in the Appalachian foreland fold and thrust belt. Our approach includes a structural analysis of shear zones and a systematic fluid inclusion study of the different minerals in veins within these shear zones.

P–T conditions related to shear zone development are conventionally determined by analysis of mineralogical assemblages using isotope and microprobe data, microtextures and fluid inclusions. Shear zone settings fall in three categories: (a) ductile shear zones in high-grade metamorphic rocks (mostly along retrogressed zones in granulitic rocks), (b) dominantly brittle–ductile shear zones in low- to medium-grade metamorphic rocks (greenschist to lower amphibolite facies rocks),

[1] Present address: Department of Each Sciences, University of Roorkee, Roorkee – 247667, U.P., India.

0040-1951/91/$03.50

Fig. 2. Z-shaped en-echelon veins in the dextral shear zones (length of the pencil: 12 cm).

of brittle–ductile shear zones containing en-echelon arrays of extension veins are well exposed. In general, the shear zone thickness (perpendicular to shear zone walls) varies from 10 to 30 cm and they extend along their strike for less than 2 m. These shear zones can be classified in two sets (I and II) on the basis of the sense of shearing and, the orientation of veins and shear zones. NNW-striking set-I shear zones dip at 70–80° towards ENE and contain lensoid and Z-shaped en-echelon veins, indicating dextral shearing (Figs. 2 and 3). Set-II shear zones also strike NNW–SSE but they

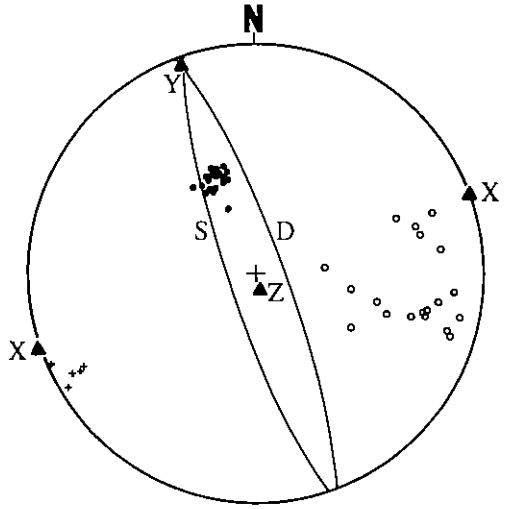

Fig. 3. Lower-hemisphere projection (great circle) of the mean orientations of sinistral (S) and dextral (D) shear zones (triangles are orientations of the principal axes of bulk strain ellipsoid, $X \geq Y \geq Z$; pluses and circles are poles to the orientation of veins in dextral and sinistral shear zones respectively; dots = poles to bedding).

dip towards WSW (Fig. 3) and contain lensoid and S-shaped en-echelon veins suggesting sinistral shearing. In outcrops, where set-I and set-II shear zones occur together, it is impossible to establish a distinct or consistent overprinting relationship between the two. Several lines of evidence including the consistently opposite sense of shearing in set-I and set-II shear zones; common strike of both the sets of shear zones and corresponding veins and; the parallelism of set-I shear zones with the veins in set-II shear zones and vice-versa, suggest that shear zones of set I and set II have formed synchronously as conjugate pairs.

As the dextral (I) and sinistral (II) sets of shear zones are equally well developed, their geometry can be used to determine the orientation of bulk strain ellipsoid ($X \geq Y \geq Z$). The underlying principle behind such analysis assumes that the conjugate shear zones intersect along the intermediate axis (Y) and, the acute and obtuse bisectors of the angle between conjugate pair define Z and X axes respectively (Ramsay and Huber, 1987). Strain analysis reveals that the bulk strain ellipsoid for brittle–ductile shear zones considered here can be defined by subhorizontal X and Y axes trending towards ENE and NNW respectively (Fig. 3). The Z axis of finite strain ellipsoid defining the direction of maximum shortening was oriented subvertically. In addition, the low angles ($< 45°$) between shear zone wall and veins ($\approx$ 35–40° in sinistral and $\approx 25°$ in dextral shear zones) and, acute dihedral angles ($\approx 20°$) suggest increase in volume or positive dilation during the course of deformation with strike-parallel stretching (Fig. 3).

Internal geometry and composition of veins

Typical en-echelon veins in both dextral and sinistral shear zones are characterized by three mineralogically different zones arranged parallel to the vein boundaries. Each vein is primarily made up of a pink median zone bounded symmetrically on either side by marginal zones of white calcite (Fig. 4a). Contacts between these zones are characterized by the occurrence of wall-rock inclusion bands and euhedral quartz crystals. Staining with alizarin red shows that the pink and white

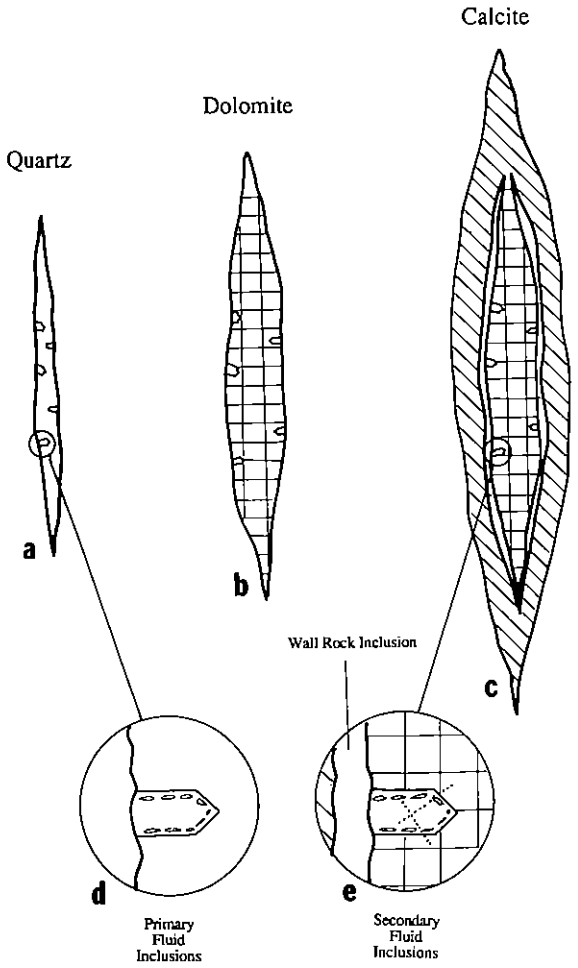

Fig. 5. Schematic diagrams showing successive precipitation of quartz, saddle dolomite and calcite in the en-echelon, extension veins within shear zones. Average length of vein in Fig. 5c varies between 10 and 20 cm.

was precipitated later than the saddle dolomite. In summary, quartz, saddle dolomite and calcite crystallized in paragenetic order within the extension veins of the investigated shear zones.

Fluid inclusions

Types of fluid inclusions

Euhedral crystals of quartz, saddle dolomite and calcite were mechanically separated for the purpose of fluid inclusion analysis of individual minerals in the multimineralic extension veins within shear zones. Petrographic studies on doubly-polished plates revealed the presence of two types of fluid inclusions in all the minerals (Fig. 4d). Type-I (two phase) fluid inclusions were characterized by more than 80–90% liquid phase and a small but distinct vapor bubble at room conditions. Type-II (mono-phase) fluid inclusions were typically dark colored, negative crystal shaped and did not exhibit any observable vapor phase (vapor bubble) at room conditions. In euhedral quartz crystals, the fluid inclusions were mostly of large size (10–30 μm) and optically more clear. On the contrary, the fluid inclusions in dolomite and calcite were very small (< 5–10 μm) and turbid in appearance. In all the samples, crushing stage tests showed presence of numerous gas bubbles which dissolve in kerosene suggesting occurrence of light hydrocarbon (methane) in both the types of fluid inclusions. On the basis of crushing stage experiments we have inferred that type-I (two-phase) and type-II (mono-phase) represent water-rich and methane-rich fluid inclusions respectively.

We have considered only those fluid inclusions as primary which occurred in arrays parallel to crystal boundaries in quartz and growth zones in dolomite and calcite (Fig. 5d). All other fluid inclusions, particularly those occurring along transgranular arrays, were considered to be secondary (Fig. 5e). It was commonly found that the type-I (two phase) and type-II (mono-phase) fluid inclusions occurred along the same trail parallel to crystal boundaries or growth zones suggesting the synchronous trapping of type-I and type-II fluid inclusions of the primary origin. Due to very small sizes (< 3 μm) of secondary fluid inclusions, particularly in saddle dolomite and calcite, most of the microthermometric data presented in this paper have been generated by observations on the primary inclusions. In quartz, however, type-I (two phase) primary inclusions exhibited large variations in size and liquid/vapor ratios at room conditions due to post-enetrapment changes such as stretching, necking and resealing of fluid inclusions. Bodnar et al. (1985) have demonstrated that, although these post-entrapment phenomena have little or no effect on the salinity of the fluids, they cause very erroneous estimates of homogenization and consequently trapping temperatures. Therefore, in our experiments, the use of primary inclusions (type I) in quartz was restricted to

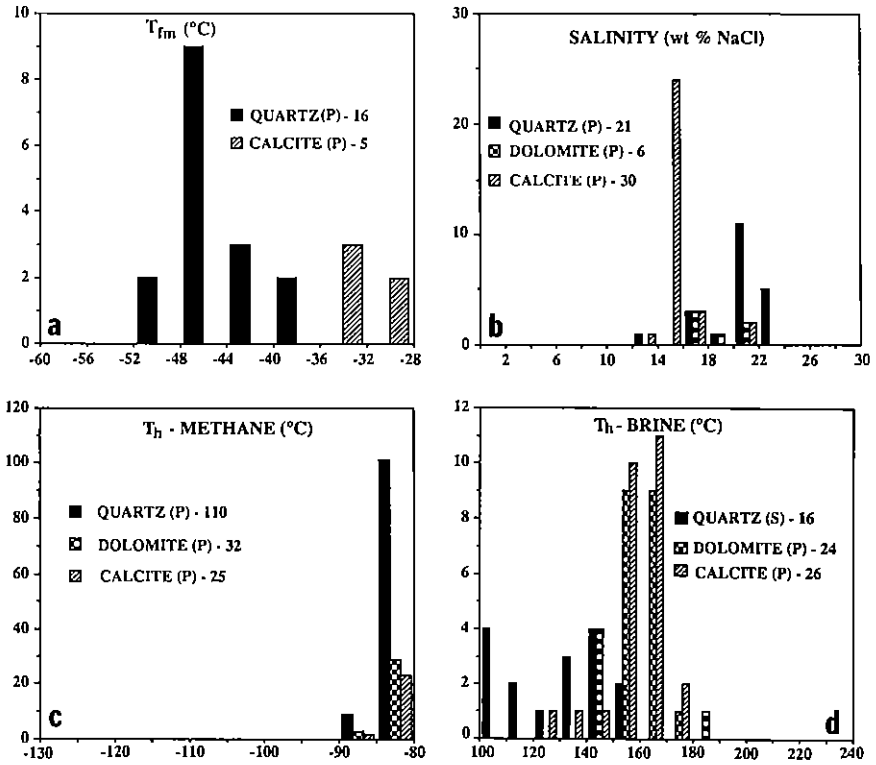

Fig. 6. Frequency histograms representing data on microthermometric measurements. T_{fm} = temperature of first melting in the type-I inclusions; T_h-*METHANE* = homogenization temperature of methane in type-II inclusions; T_h-*BRINE* = homogenization temperature of in type-I inclusions; *P* and *S* = data on primary and secondary fluid inclusions respectively. Numbers = total number of the observations.

calcite, the salinity of these complex brines went down from 19–17 wt.% NaCl to about 15 wt.% NaCl.

In type-II (mono-phase fluid inclusions, cooling below −80 °C resulted in the appearance of a vapor bubble which grew larger in size with further lowering of the temperature. In few inclusions, the vapor bubble displayed a distinct jerk at temperatures ranging from −150 °C to −140 °C to indicate the freezing of CO_2. At extremely low temperatures, approximately −194 °C, these fluid inclusions were characterized by large vapor bubble showing sharp and angular boundaries. On slow heating, the sharp and angular boundaries of vapor bubble changed with a sudden jerk, to smooth and rounded boundaries. This event marked the final melting of solid methane (T_m-methane) at temperatures ranging from −183 °C to −178 °C. In fluid inclusions containing carbon dioxide, the last crystal of CO_2 melted between −120 °C to −103 °C. Finally, in all type-II inclusions, the vapor bubble homogenized into liquid phase at temperatures ranging from −89 °C to −83 °C (Fig. 6c).

The above microthermometric data strongly suggest a methane-rich composition of type-II inclusions. Any possibility of the presence of nitrogen in these inclusions is ruled out as the final melting of methane occurs around its triple point (−182.47 °C). Similarly, low melting temperatures (−120 °C to −103 °C) of CO_2 suggest that the amount of CO_2 present in these inclusions is less than 2% of the total volume of the inclusion. From these results, it is therefore inferred that type-II fluid inclusions are compositionally more than 98% pure methane. Consequently, we have used

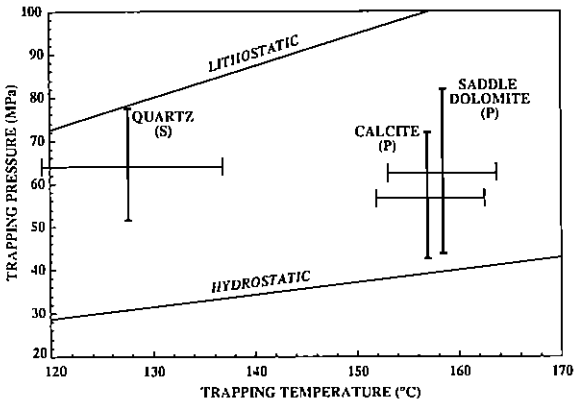

Fig. 7. Trapping conditions for fluids in quartz, saddle dolomite and calcite (P and S = primary and secondary fluid inclusions respectively; horizontal bars = standard deviations about the mean trapping temperatures; vertical bars = range of the trapping pressures of fluids; upper and lower ends of the vertical bars = maximum and minimum trapping pressures respectively). The hydrostatic and lithostatic gradients have been calculated assuming a geothermal gradient of 27 °C/km.

in quartz during the late stage of vein formation (Fig. 5e).

Trapping pressures

On a P–T graph, the intersection of an isochore corresponding to a given density of methane and a line parallel to the pressure axis at mean homogenization temperature gives the trapping pressure (T_h-isochore intersection method; Fig. 7). Our results reveal a wide range of methane densities due to large variations in the homogenization temperature of the type-II fluid inclusions. One possibility is that variations in the homogenization temperature are due to post-entrapment changes. We rule this out on the basis of two lines of evidence. First, for a given sample, the type-I inclusions show consistent homogenization temperatures (T_h-brine) proving that these inclusions have not suffered post-entrapment changes. In view of the co-existence of type-I and type-II inclusions, it is unlikely that type-II inclusions underwent post-entrapment changes while the type I escaped these effects. Second, within smaller domains of a growth zone, both type-I and type-II inclusions homogenized at reasonably consistent homogenization temperatures (T_h-brine and T_h-methane). Therefore, the large variation in the homogenization temperature of type-II (monophase) inclusions should reflect the trapping of fluids at varied pressures.

In the absence of evidence to establish the chronology of successive growth zones, it was not possible to ascertain the pressure fluctuations between successive growth zones in individual minerals (Mullis, 1975). We have used the maximum and minimum homogenization temperatures (T_h-methane) to calculate the isochores corresponding to the two extreme values of densities. The line of mean homogenization temperature of type-I fluid inclusions intersects these two extreme isochores at two points defining the maximum and minimum trapping pressures (Fig. 7).

We attribute the large fluctuations in trapping pressure at isothermal conditions to the crack-seal mechanism of vein development in the brittle–ductile shear zones. This mechanism is characterized by the formation and healing of extension fractures (mode-I cracks) in episodic manner. Fluid inclusion data indicate that during each episode of crack development, the fluid pressures approached the peak trapping pressure and the subsequent healing of cracks (by precipitation of quartz, dolomite and calcite) occurred at lower pressures (Fig. 7). Thus, the peak and minimum trapping pressures obtained by fluid inclusion analyses represent the highest (70–80 MPa) and lowest (40 MPa) pressures achieved between the episodes of cracking and complete sealing by the growth of saddle dolomite and calcite in the extension veins. In quartz, the late microcracks were developed and healed at 78 MPa and 52 MPa respectively.

Discussion

Within the Coburn limestones of the Valley and Ridge, the outcrop scale shear zones have developed by brittle–ductile mechanism and progressively non-coaxial shear. Shearing was enhanced by the development of high pore pressures and decrease in effective normal stress leading to the propagation of hydraulic fractures (mode-I cracks) forming channelways for hot brines with Na^+, Ca^{2+} cations and dissolved methane. As cracking resulted in the release of pressure, the

1984; Guha and Kanwar, 1987 and; Klemd et al., 1989). It is possible that the methane bearing fluids were generated by degradation of organic matter present in or near the Coburn Formation. As a consequence of the increased generation of hydrocarbons, the pore fluid volume dilated continually until the pore pressure exceeded the least compressive stress.

Conclusions

This study demonstrates that the brittle–ductile shear zones in unmetamorphosed sediments develop at much lower pressure (80–40 MPa) and temperature (155–165°C) in comparison to shear zones in low- to medium and high-grade metamorphic rocks. Contrary to the shear zones in high-grade metamorphic rocks where CO_2 rich fluids of deep seated origin play important roles in deformation, the fluids in brittle–ductile shear zones hosted by unmetamorphosed sediments are locally derived, methane-rich brines. Fluid inclusion work further shows that the progressive evolution of the shear zones can be correlated with the systematic changes in the composition and salinity of brines precipitating different minerals in the successively formed cracks. Lastly, the crack-seal mechanism for the development of extension veins is characterized by large fluctuations in pressure under isothermal conditions.

Acknowledgements

Alfred Lacazette and Eric Beam helped in field work and fluid inclusion experiments. O.P. Varma, A.K. Awasthi, M.S. Pandian and R.M. Manickavasagam critically read the manuscript and suggested several improvements. Constructive comments from R. Jamieson and the anonymous referee helped improving the manuscript to great extent. The work was funded by post-doctoral fellowship of the Government of India to Srivastava and EPRI contract No. 25556-24 to Engelder.

References

Anderson, J.L., Robert, H.O. Palmer, D.F., 1983. Cataclastic rocks of the San Gabriel fault—an expression of deformation at deeper crustal levels in the San Andreas fault zone. Tectonophysics, 98: 209–251.

Angus, S. Armstrong, B. and de Reuck, K.M., 1976. International Thermodynamic Tables of the Fluid State—5: Methane. (International Union of Pure and Applied Chemistry, Chemical Data Ser. 16. Pergamon, New York, 247 pp.

Beach, A., 1973. The mineralogy of high temperature shear zones at Scourie, N.W. Scotland. J. Petrol., 14: 231–248.

Beach, A. and Fyfe, W.S., 1972. Fluid transport and shear zones at Scourie, Sutherland: Evidence of Overthrusting? Contrib. Mineral. Petrol., 36: 175–180.

Behr, H.J. 1980. Polyphase shear zones in granulite belts along the margin of the Bohemian Massif. J. Struct. Geol., 1/2: 249–254.

Bodnar, R.J., Reynolds, T.J. and Kuehn, C.A., 1985. Fluid-inclusion systems in epithermal systems. In: B.R. Berger and P.M. Betheke (Editors), Geology and Geochemistry of Epithermal systems. Rev. Econ. Geol., 2: 73–96.

Brethe, D., Choukroune, P. and Jegouzo, P., 1979. Orthogneiss, mylonite and non-coaxial deformation of granites: the example of the South Armocrican shear zone. J. Struct. Geol., 1: 31–42.

Burruss, R.C., 1981. Hydrocarbon fluid inclusions in studies of sedimentary brines. In: L.S. Hollister and M.L. Crawford (Editors), Short Course in Fluid Inclusions: Applications to Petrology. Mineralogy. Mineralogical Association of Canada, pp. 138–156.

Davis, G.A., 1988. Rapid upwards transport of mid-crustal mylonitic gneisses in the footwall of a Miocene detachment fault, Whipple Mountains, southeastern California. Geol. Rundsch., 77/1: 191–209.

Goldstein, A.G., 1982. Geometry and kinematics of ductile faulting in a portion of the Lake Char mylonite zone, Massachusetts and Connecticut. Am. J. Sci., 282: 1378–1405.

Guha, J. and Kanwar, R., 1987. Vug brines–fluid inclusions: a key to the understanding of secondary gold enrichment processes and the evolution of deep brines in the Canadian Shield. In: P. Fritz and S.K. Frape (Editors), Saline Water and Gases in Crystalline Rocks. Geol. Assoc. Can., Spec. Pap., 33: 95–101.

Guha, J., LeRoy, J. and Guha, D., 1979. Significance of fluid phases associated with shear zone Cu–Au mineralization in the Dore lake Complex. Chibougamau, Quebec. Bull. Minéral., 102: 569–576.

Hancock, P.L., Al-Kadhi, A., Barka, A.A. and Bewan, T.W., 1987. Aspects of analyzing brittle structures. Ann. Tectonicae, 1: 5–19.

Hanor, J.S., 1980, Dissolved methane in sedimentary brines: a potential effect on the PVT properties of fluid inclusions. Econ. Geol., 75: 603–617.

House, W.M. and Gray, D.W., 1982. Cataclasites along the Saltville thrust, U.S.A. and their implications for thrust-sheet development. J. Struct. Geol., : 257–269.

Jamieson, R.A., 1986. P–T paths from high temperature shear zones beneath ophiolites. J. Metamorph. Geol., 4: 3–22.

Klemd, R., Hallbauer, D.K. and Barton, J.M. Jr., 1989. Fluid inclusion studies of hydrothermally altered Archean granites around the Witwatersand basin. Mineral. Petrol., 40: 39–56.

Losh, S., 1989. Fluid–rock interaction in an evolving ductile shear zone and across the brittle–ductile transition, central Pyrenees, France. Am. J. Sci., 289: 600–648.

McCaig, A.M., 1984. Fluid–rock interaction in some shear zones from the Pyreens. Jr. Metamorph. Geol., 2: 129–141.

McCallum, M.E., 1974. Dedolomitized marble lenses in shear zone tectonics, Medicine Bow Mountains, Wyoming. J. Geol., 82: 473–487.

Means, W.D., 1976. Stress and Strain: Basic Concepts of Continuum Mechanics for Geologists. Springer, New York, 339 pp.

Mullis, J., 1975. Growth conditions of quartz crystals from Val d'Illiez (Valais, Switzerland). Schweiz. Mineral. Petrogr. Mitt., 55: 419–429.

Mullis, J., 1987. Fluid inclusion studies during very low-grade metamorphism. In:M. Frey (Editor), Low Temperature Metamorphism. Blackie, Glasgow, pp. 162–199.

O'Hara, K., 1988. Fluid flow and volume loss during mylonitization: an origin for phyllonite in an overthrust setting, North Carolina, U.S.A. Tectonophysics, 156: 21–36.

Pollard, D.D. and Aydin, A. 1988. Progress in understanding jointing over the past century. Geol. Soc. Am. Bull., 100: 1181–1204.

Radke, B.M. and Mathis, R.L., 1980. On the formation and occurrence of saddle dolomite. J. Sediment. Petrol., 50: 1149–1168.

Raith, M., Hengest, C., Nagel, B. and Bhattacharya, A., 1988. Metamorphic conditions in the Nilgiri granulite terrane and the adjacent Moyar and Bhavani shear zones: a reevaluation (abstr.). Workshop on the deep continental crust of south India, Geological Society of India, 112–113.

Ramsay, J.G., 1980a. Shear zone geometry, a review. J. Struct. Geol., 1/2: 83–99.

Ramsay, J.G., 1980b. The crack-seal mechanism of rock deformation. Nature, 284: 137–139.

Ramsay, J.G. and Huber, M.I., 1987. The techniques of Modern Structural Geology, vol. 2. Fold and Fractures. Academic Press, London, pp. 309–700.

Robert, F. and Kelly, W.C., 1987. Ore-forming fluids in Archean gold-bearing quartz veins at Sigma mine, Abitibu greenstone belt, Quebec, Canada. Econ. Geol., 82: 56–74.

Roedder, E., 1984. Fluid Inclusions: Reviews in Mineralogy. Mineralogical Society of America, Washington, D.C., 12: 646 pp.

Shepherd, T.J., Rankin, A.H. and Alderton, D.H.M., 1985. A Practical Guide to Fluid Inclusion Studies. Blackie, Glasgow and London, 239 pp.

Sibson, R.H., 1989. Earthquake faulting as a structural process. J. Struct. Geol., 11: 1–14.

Srivastava, D.C. and Engelder, T., 1990. Crack-propagation and pore-fluid conditions during fault bend folding in the Appalachian Valley and Ridge, Central Pennsylvania. Geol. Soc. Am. Bull., 102: 116–128.

fluids became immiscible into methane-rich and water-rich components. Furthermore, we presume that the sudden and substantial drop in pressure during crack propagation resulted in the decrease of solubility of the silicates and carbonates. As a consequence, quartz, saddle dolomite and calcite were precipitated in open spaces created by cracking. The evolution of shear zones was marked by a minimum of three such crack-seal episodes demarcated by the successive deposition of quartz, saddle dolomite and calcite. The sequence of mineral infillings in veins, commencing from quartz, through saddle dolomite, to calcite is remarkably consistent in each multimineralic vein of any given shear zone.

The composition of fluids changed during the progressive evolution of shear zones. In general, the fluids diluted from 23 wt.% NaCl during the precipitation of quartz to 15 wt.% NaCl during the growth of calcite. It is further evident that the different minerals crystallized at narrow ranges of temperature (155–165°C) but under large pressure fluctuations (80–40 MPa). This evidence suggests that the shear zones evolved at nearly isothermal conditions accompanied by the wide fluctuations in the pressure ($\Delta P_p \approx 40$ MPa).

For the Spruce Creek area, Srivastava et al. (unpublished) have calculated a geothermal gradient of 27°C/km on the basis of fluid inclusion data from bedding parallel veins in the Coburn Formation and an overburden thickness of 6.5 km. Using this geothermal gradient, we have plotted lithostatic (26 MPa/km) and hydrostatic (10 MPa/km) thermobaric gradients on a P–T diagram illustrating the trapping conditions of fluids (Fig. 7). The maximum trapping pressure obtained from fluid inclusion analysis is less than lithostatic pressure (Fig. 7) suggesting the propagation of mode-I cracks in shear zones at sublithostatic pressures.

The paradoxical situation of the propagation of mode-I cracks at sub-lithostatic pressure is explained by a model where steep cross-fold veins develop due to stretching of beds parallel to strike, on the hanging-wall side of the thrust surface during fault-bend folding (Srivastava and Engelder, 1990). As the Coburn Formation at Spruce Creek is located on the hanging-wall side of the Yellow Spring thrust, we infer that the steep shear zone veins (close in orientation to cross-fold veins) have developed during the ramping of Coburn beds along the Yellow Spring thrust. This inference is supported by shear zone analysis revealing that the direction of maximum elongation (X) is parallel to the strike of the beds at Spruce Creek. We, therefore, attribute the development of extension veins and shear zones to the stretching of beds parallel to strike direction (ENE) during thrusting.

Unlike horizontal fractures, the pore fluid pressure need not approach or exceed the lithostatic pressure for the propagation of steep fractures. This fact is supported by fluid inclusion data which show that the peak trapping pressure during the development of NNW–SSE striking and steeply dipping shear zone veins was below lithostatic pressure (Fig. 7). The lower limit of trapping pressure approached sub-hydrostatic pressure at which the saddle dolomite and calcite were precipitated to completely seal the open fractures.

The orientations of the local maximum (σ_1) and minimum (σ_3) principal stress axes are constrained by the thrust fault regime of the area and steep dips of the extension veins, respectively. Therefore, the local stress ellipsoid responsible for the development of shear zones can be defined by subhorizontal σ_3 and σ_1 axes trending NNE–SSW and NNW–SSE, respectively, and subvertical intermediate stress axis (σ_2). Results of this study suggest that the orientations of X, Y, and Z-axes determined by shear zone analyses did not coincide with the orientations of local σ_3, σ_2 and σ_1 axes, respectively. This non-coincidence of the principal axes of stress and strain ellipsoids is attributable to the non-coaxial nature of deformation (Hancock et al., 1987; Means, 1976).

Evidence, such as the localized nature of shear zones; their restricted lateral and vertical extents (few centimeters to a couple of meters) and; their confinement to carbonate beds of a few meters thickness, imply that the source for fluids is likely to be local. This inference is also corroborated by fluid inclusion results revealing highly saline fluids containing methane and cations like Na, Ca and Mg. Such fluids may owe their origin to connate water and/or modified formation water (Roedder,

the equation of state for pure methane (Angus et al., 1976) to calculate the density and isochores of type-II inclusions.

Heating experiments

Heating experiments were carried out only on type-I inclusions, to measure the homogenization temperatures (T_h-brine). These inclusions were primary in saddle dolomite and calcite and secondary in quartz. A minimum accuracy of $\pm 3°C$ was achieved during the measurement of homogenization temperatures (T_h-brine). On progressive heating of a typical type-I inclusion, the vapor bubble was observed gradually reducing in size until it totally disappeared upon homogenization with the liquid phase. None of the type-I inclusions showed homogenization into vapor phase or critical homogenization. Three precautions were taken to avoid the effects of necking and stretching during the heating runs (Roedder, 1984). First, only those groups of fluid inclusions which exhibited consistent liquid/vapor ratios at room temperature were heated to obtain the data on homogenization temperature. Second, in any particular doubly-polished plate placed under the heating-freezing stage, the T_h measurements were made in the ascending order of homogenization temperature. Third, on any single chip under the stage, the number of T_h observations were restricted to less than ten in order to avoid thermal stretching due to repeated heating. In general, all the type-I inclusions homogenized into liquid phase at temperatures between 100°C to 185°C (Fig. 6d).

Thermobarometry

All the three minerals (quartz, saddle dolomite and calcite) comprising extension veins in shear zones contained both water-rich (type I) and methane-rich fluid inclusions (type II). As both these types of fluid inclusions were observed within the same petrographic feature, such as growth zones or microfractures, we infer that methane-rich and water-rich fluid inclusions were trapped simultaneously and, the water-rich fluid inclusions were saturated with methane. The simultaneous trapping of type-I and type-II inclusions is reaffirmed by reasonable consistencies in homogenization temperatures of type-I (T_h-brine) and type-II (T_h-methane) fluid inclusions occurring within same growth zone. Considering the fact that water-methane saturation occurs at homogenization conditions, the homogenization temperature of methane-saturated, water-rich fluid inclusions (type I) is the trapping temperature.

When the methane-rich and water-rich fluid inclusions co-exist, three different methods are commonly applicable for geobarometry, viz. (a) the isochore intersection method, (b) the T_h-isochore intersection method and (c) the methane–water saturation method (Mullis, 1987). A critical evaluation and comparison of these methods by Mullis (1987) has revealed that the "T_h-isochore intersection method" yields the best estimates of trapping pressure. This is due to the fact that this method does not require any pressure correction, which if applied in case of methane-bearing inclusions, gives erroneously high trapping temperature (Hanor, 1980; Burruss, 1981; Mullis, 1987).

Trapping temperatures

Following the principles of geothermometry outlined in the preceding section, the homogenization temperature of type-I inclusions represent the trapping temperature. In saddle dolomite and calcite, these inclusions homogenized at temperatures ranging from 130°C to 190°C. The modal values of this range of temperature lie between 155°C and 165°C and represent the trapping temperature of the fluids that precipitated saddle dolomite and calcite during the vein growth in shear zones. It was not possible to estimate the temperature of fluids trapped during the growth of quartz because primary type-I inclusions exhibited large variations in size and liquid/vapor ratios due to stretching and necking. Quartz crystals, however, contained workable sizes of (≥ 5 μm) of secondary type-I (two phase) inclusions along the microfractures. These secondary inclusions homogenized at temperatures ranging from 100°C to 152°C (with mean at 128°C; Fig. 6d). It is evident that these temperatures represent the healing temperatures in the micro-cracks formed

measurements of freezing point depressions only and no heating runs were performed on them.

Freezing experiments

Freezing experiments were made on primary (type-I and type-II) inclusions in quartz, saddle dolomite and calcite, using a modified U.S.G.S. type of gas flow heating–freezing stage manufactured by Fluid Inc. For type-I (two phase) fluid inclusions, the temperatures of first melting (T_{fm}) and final melting (T_m) are precise to $\pm 3°C$ and $\pm 1°C$ respectively. In case of type II (mono-phase) inclusions, the temperatures of final melting of methane (T_m-methane), final melting of carbon dioxide ($T_m - CO_2$) and, the homogenization of methane (T_h-methane) are precise within the ranges of $\pm 8°C$, $\pm 5°C$ and $\pm 3°C$ respectively. The generalized heating–freezing characteristics of type-I and type-II fluid inclusions are represented in Table 1.

Progressive cooling of type-I inclusions resulted in sudden jerk or collapse of vapor bubble marking the complete freezing of fluid. Subsequently, on slow warming the appearance of a very granular texture demarcated the first melting of ice crystals (T_{fm}) at the eutectic temperature of the salt–water system (Shepherd et al., 1985). As the range of observed T_{fm} temperatures ($-30°C$ to $-50°C$) is much lower than the eutectic temperature ($-20.8°C$) of the H_2O–NaCl system, the presence of bivalent cations (Ca and Mg) in type-I fluid inclusions is indicated (Fig. 6a). On further heating, the remaining crystals of ice gradually melted and the melting temperature of the last ice crystal was carefully recorded to mark the freezing point depression (T_m-brine). T_m-brine was recorded either by direct observation on the melting of last ice crystal or by a cycling technique, the latter applied mostly to small inclusions ($< 5\ \mu m$) in the saddle dolomite and calcite. The conversion of data on freezing point depression (T_m-brine) to wt.% equivalent NaCl salinities reveals that the oldest mineral quartz was precipitated by the most saline brines (23–21 wt.% NaCl; Fig. 6b). During the subsequent growth of saddle dolomite and

TABLE 1
Summary of the heating–freezing characteristics of fluid inclusions

F.I. type	T range (°C)	Observation	Interpretation
Type-I (two-phase) methane saturated water-rich fluid inclusions	−50 to −70	Collapse of vapor bubble with sudden jerk	Complete freezing of fluid
	−30 to −50	Very granular texture	Eutectic temperature (T_{fm})
	−8 to −20.5	Melting of the last ice crystal	Freezing point depression (T_m)
	+100 to +185	Disappearance of vapor bubble	Homogenization temperature (T_h-brine)
Type-II (mono-phase) methane-qrich fluid inclusions	⩽ −190	Sharp and angular boundaries of the vapor bubble	Freezing of methane
	−183 to −178	Rounding and smoothening of vapor bubble boundaries with sudden jerk	Freezing point depression of methane (T_m-methane)
	−120 to −102	Gradual melting of the last crystal of CO_2	Melting temperature of CO_2 ($T_m = CO_2$)
	−89 to −83	Disappearance of of vapor bubble	Homogenization temperature of methane (T_h-methane)

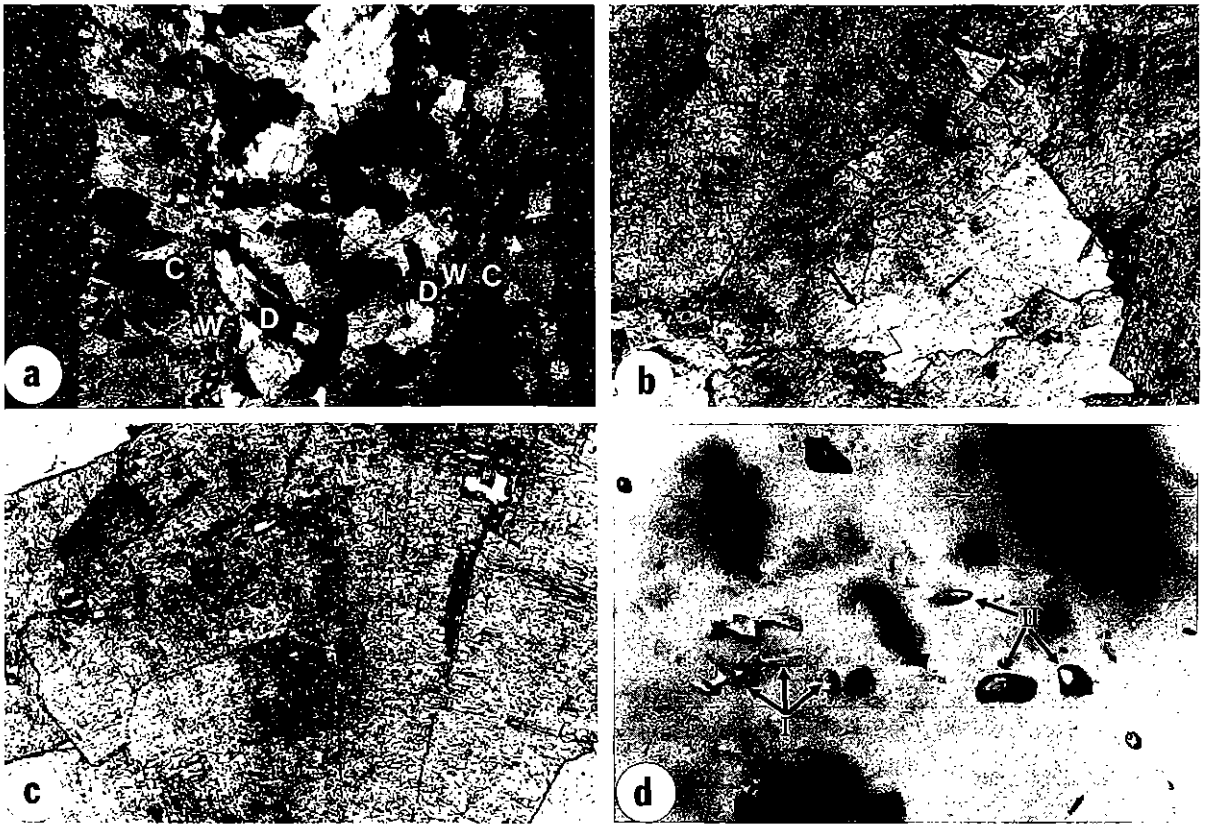

Fig. 4. (a) Photomicrograph showing geometry and mineralogy of a typical extension vein in shear zone. Crossed nicols, field of view 5 × 7 mm; C = calcite; W = wall-rock inclusion band; D = saddle dolomite). (b) Photomicrograph showing growth zones (indicated by arrow) parallel to the boundary of spear shaped grain of the saddle dolomite. Crossed nicols; field of view 2.5 × 3.8 mm. (c) Photomicrograph showing curved cleavages in saddle dolomite. Crossed nicols; field of view 2.5 × 3.8 mm. (d) Photomicrograph showing the occurrence of type-I (two-phase) and type-II (mono-phase) fluid inclusion. Uncrossed nicols, field of view 0.3 × 0.5 mm.

carbonates are dolomite and calcite zones respectively. Microscopically, the pink median zones in these veins consists of coarse (40–300 μm), spear-shaped dolomite grains showing curved crystal faces, warped cleavages, denticulate intergranular boundaries and wavy extinctions (Figs. 4b and 4c). Such characteristics imply that these grains are "saddle dolomite", commonly found in association with hydrocarbons and epigenetic mineralizations (Radke and Mathis, 1980). In contrast to the median zones of saddle dolomite, the white marginal zones are characterized by medium grained (40–100 μm) subhedral calcite crystals showing occasional microtwins.

Outcrop and petrographic evidence showing the lack of lateral offset in the pre-existing bio-markers and veins across the shear zone veins suggest their development by mode-I cracking (Pollard and Aydin, 1988). Furthermore, the occurrence of wall-rock inclusion bands at both the contacts between the median zone of saddle dolomite and the marginal zones of calcite indicate the formation of these veins by successive crack-seal events (Ramsay, 1980b). The first event resulted in the growth of euhedral quartz crystals in the open space created as a consequence of the earliest episode of mode-I cracking (Fig. 5a). Further fracturing resulted in the enlargement of open spaces and their infillings by saddle dolomite (Fig. 5b). The last crack-seal event included fracturing along the contacts of saddle dolomite and host rock, and the subsequent sealing by precipitation of white calcite (Fig. 5c). As a rule, thin late offshoots of the main extension veins are devoid of saddle dolomite and consist entirely of white calcite only. This geometrical evidence reaffirms that the calcite

and (c) brittle to brittle–ductile shear zones in very low-grade metamorphic or unmetamorphosed sediments. In high-grade (granulitic) rocks, the deformation leading to shear zone development takes place at 600–900 °C temperature, 600–900 MPa pressure and the syntectonic fluids are CO_2 rich brines of deep seated origin (Beach and Fyfe, 1972; Beach, 1973; Behr, 1980; Goldstein, 1982; Raith et al., 1988). In general, shear zones in low- to medium-grade metamorphosed rocks develop through the influx of low salinity brines ($\pm CO_2$) at temperatures ranging from 200 °C to less than 500 °C and pressures varying from 200 MPa to less than 500 MPa (McCallum, 1974; Brethe et al., 1979; McCaig, 1984; Jamieson, 1986; Robert and Kelly, 1987; Davis., 1988; O'Hara, 1988; Losh, 1989; Sibson, 1989). Low-pressure fluid inclusions are found in Au–Cu mineralized, brittle–ductile shear zones in granite–greenstone terrain of Quebec (Guha et al., 1979; Guha and Kanwar, 1987). The mineralizing fluids in these shear zones are highly saline brines co-existing with methane-rich fluids trapped at 240 °C and 80 ± 0.5 MPa.

P–T data on brittle and brittle–ductile shear zones developed in very low-grade metamorphic or unmetamorphosed sediments are very scarce. On the basis of zeolite facies assemblage, Anderson et al. (1983) deciphered the development of the San Gabriel fault (brittle shear zone) at 200 ± 30 °C temperature and 2–5 km depth. Similarly, microstructural studies in the Appalachian foreland fold and thrust belt have revealed the development of cataclasites in Saltville thrust at 250 °C temperature and 65–130 MPa pressure (House and Gray, 1982). In this paper, we present the P–T conditions for the development of brittle–ductile shear zones in the unmetamorphosed carbonates in the Appalachian Valley and Ridge.

Geometry and analysis of shear zones

The brittle–ductile shear zones discussed in this paper are hosted by the Ordovician Coburn Formation exposed along Spruce Creek in the Valley and Ridge of central Pennsylvania (Fig. 1). At this locality, the Coburn Formation comprises a sequence of predominantly bio-micritic limestones and dolomites. With reference to the regional structure, these outcrops define the closure region of a low plunging fold located on the hanging wall of Yellow Spring thrust (Figs. 1b). Dip of beds in the outcrop vary from 40 ° to 55 °.

In a 100 m strike length of the Coburn Formation outcropping at Spruce Creek, about a dozen

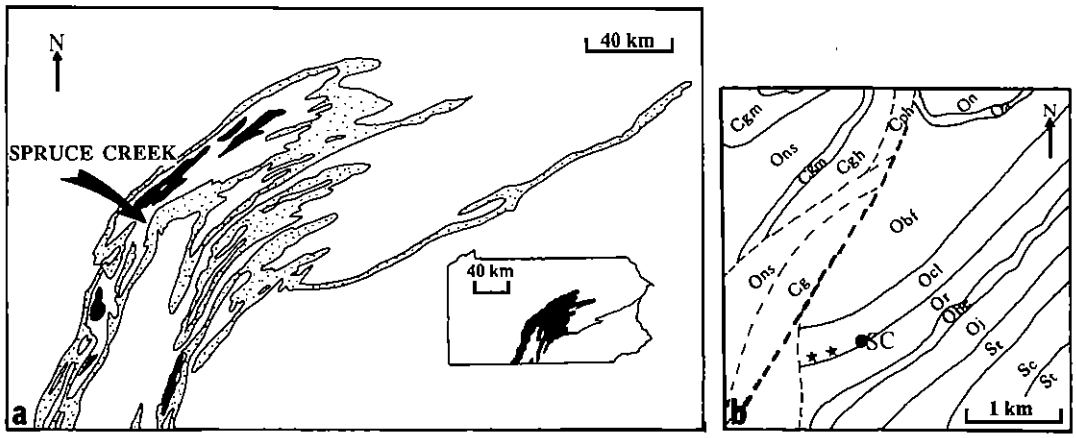

Fig. 1. (a) Location of study area in the Valley and Ridge Province of central Pennsylvania. Black = Cambrian; dots = Silurian; blank between black and dots = Ordovician. Inset shows the location of Valley and Ridge Province in Pennsylvania. (b) Geological map of the area around Spruce Creek. Continuous line = formation boundary; dashed line = fault; star = sample location and outcrops showing brittle–ductile shear zones; C_g = Gatesburg Formation; O_{ns} = Nittany and Stonehenge/Larke Formations; O_{bf} = Bellefonte Formation; O_{cl} = Coburn through Loysburg Formations; O_r = Reedsville Formation; O_{be} = Bald Eagle Formation; O_j = Juniata Formation; S_t = Tuscarora Formation; S_c = Clinton Gp.; *SC* = Spruce Creek. Fault placing O_{bf} over C_g is the Yellow Springs thrust.